JOURNAL OF MATERIALS SCIENCE 28 (1993) 1515–1524

The effect of porosity on the microstructural damping response of 6061 aluminium alloy

J. ZHANG*, M. N. GUNGOR‡, E. J. LAVERNIA*
*Materials Science and Engineering, Department of Mechanical and Aerospace Engineering, University of California at Irvine, Irvine, CA 92717, USA
‡Westinghouse Science and Technology Center, 1310 Beulah Road, Pittsburgh, PA 15235, USA

The paper reports on the results of a systematic study of the effects of micrometre-sized pores on the damping response of 6061 aluminium alloy. Spray atomization and deposition processing was utilized for the present study as a result of its ability to produce a material with a pre-determined amount of non-interconnected, micrometre-sized pores. The amount and distribution of pores present in the material may be systematically altered through variations in the processing parameters by using this synthesis approach. The damping measurements were conducted on cantilever beam specimens by using free vibration decay and resonant vibration techniques. Experimental results showed that the porosity increased with increasing average pore size; the damping capacity, in terms of logarithmic decrement δ, of the as-spray-deposited 6061 Al alloy, increased from 1.8 to 2.9% as the amount of porosity increased from 4 to 10%. Comparisons show that the damping capacity of the as-spray-deposited 6061 Al alloy is higher than those reported by other investigators using the same alloy but with different processing techniques. The loading damping mechanisms are discussed in the light of data from the characterization of microstructure and damping capacity.

1. Introduction

The effective utilization of advanced metals and alloys in structural applications that require minimal sound and vibration transmission is often limited by our existing understanding of the factors that govern their microstructural damping response. The microstructural damping capacity of a material, referred to hereafter simply as damping capacity, is defined as its ability to dissipate elastic strain energy during mechanical vibration of the material under cyclic loading, although plasticity may be involved at large strain amplitudes. The dissipation of elastic strain energy in the microstructure typically occurs through a combination of several mechanisms. Among the damping mechanisms that are important in metals and alloys, thermoelasticity effects and microstructural effects (e.g. crystallographic defects) are the two main contributors to material damping under conventional conditions, although other damping mechanisms such as eddy-current effects, Snoeck effects, stress-induced ordering reactions and electronic effects may induce damping peak phenomena under certain temperature, strain amplitude and frequency conditions [1]. Thermoelastic damping can be described by the fact that thermal conductivity provides the mechanism of relaxation in metals, whereas microstructural defects contribute to damping by dissipating energy during their movement and interaction. The defects inside polycrystalline metals and alloys include point defects (vacancies and disorders), line defects (dislocations), surface defects (grain boundaries and interfaces) and bulk defects (micro-pores and micro-cracks). It has been shown that mobility of point defects and dense dislocations give intermediate damping, while sliding along grain boundaries and bulk defects are responsible for high damping capacity [2–5].

Experimental evidence has demonstrated that the presence of pores or cavities in some non-metallic materials may play an important role in the damping response of the material. Shimizu [3], for example, showed that the damping behaviour of a carbon–epoxy composite could be modified either by adding a certain amount of plasticizer or by foaming the epoxy matrix. His results demonstrated that the damping behaviour of the carbon–epoxy composite samples was strongly influenced by the resulting porous microstructure that was induced during the foaming of the matrix. In related studies, Klimentos and McCann [4] investigated the relationship among compressional wave attenuation, porosity, clay content and permeability in sandstones. In their study, they measured the attenuation coefficients of compressional waves in sandstone samples containing pores filled with clay and saturated with some type of fluid. Their results showed that the logarithmic decrement δ of the samples at 1000 kHz and 40 MPa was related to the porosity P% and the clay content inside the pores C % by $\delta = aP + bC - c$, where a, b and c are positive constants. They also noted that there was no apparent correlation between attenuation and mean grain size

0022–2461

for their samples. Nielsen [5] developed a theoretical model to estimate the complex modulus of porous and impregnated materials (e.g. cement) and viscoelastic porous materials. Rice [6] also proposed a theoretical model to predict the effects of porosity and grain size on the tensile modulus, strength and fracture energy of ceramics.

Although the aforementioned results suggest that the presence of pores and cavities may have a strong influence on the overall damping response of non-metallic materials, the role played by pores and cavities in the damping behaviour of metallic materials is not clearly understood. This lack of knowledge may limit the efficient use of certain advanced materials in damping-critical structures, since these materials often exhibit some porosity. One such class of materials includes that produced by powder metallurgical means (consolidating fine powders into bulk preforms) [7, 8]. In addition, more or less porosity may exist in metals and alloys processed by other metallurgical techniques.

The objective of the present work is to provide insight into the effects of porosity on the damping behaviour of structural aluminium alloys. Spray atomization and deposition processing was selected for the present study as a result of its ability to produce a material with a pre-determined amount of non-interconnected, micrometre-sized pores [9–15]. Furthermore, by using this synthesis approach, the amount and distribution of pores present in the material may be systematically altered through variations in the processing parameters. 6061 aluminium alloy was selected for the present study because it has been widely used in structural applications, and because its damping behavior has been studied previously [16, 17].

2. Experimental procedure

2.1. Materials synthesis

The aluminium alloy used in the present study was a commercial quality 6061 aluminium alloy, with the following nominal composition: 0.6% Si, 0.28% Cu, 1.0% Mg, 0.2% Cr, balance Al (wt %). Spray atomization and deposition processing involves the energetic disintegration of the molten 6061 alloy into micrometre-sized droplets by high-velocity inert gas jets (N_2 was used in the present study), followed by deposition on a water-cooled Cu substrate. The rapidly quenched, partially solidified droplets impact, first on the deposition surface, and subsequently on each other, and collect into a preform whose microstructure is largely dictated by the solidification conditions during impact. A diagram of the experimental apparatus used in the present study is shown in Fig. 1. The geometry of the spray-deposited material, which normally exhibits a contour akin to the Gaussian distribution of droplets impacting on the substrate [9–13], was readily modified in the present study by displacing the substrate during deposition. In order to avoid extensive oxidation of the 6061 Al matrix during processing, the environmental chamber was evacuated to a pressure of 0.2 kPa and backfilled with inert gas to pressure of 0.1 MPa. This procedure was performed again to reduce the amount of residual oxygen inside the chamber prior to melting and atomizing the material. A more detailed discussion of the spray atomization and deposition experiments can be found elsewhere [9–15].

Two runs of spray atomization and deposition experiments using 6061 Al alloy were conducted for the present study. The primary experimental variables used during each experiment are shown in Table I. The parameters in this table show that the metal-to-

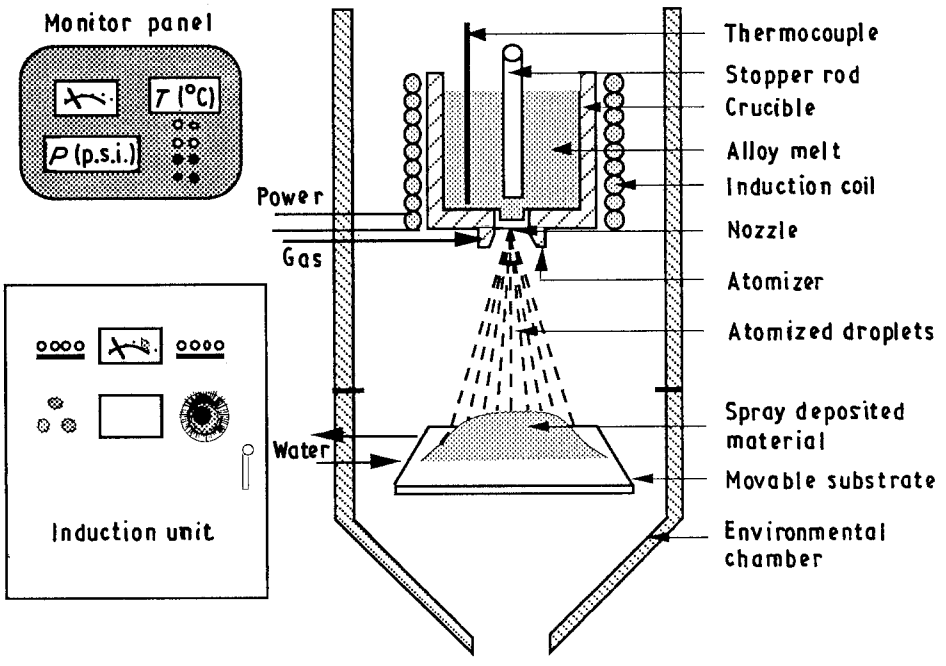

Figure 1 Schematic diagram showing spray-atomization and deposition processing.

TABLE I Experimental variables used in the study

Experiment No.	132	134
Alloy	6061 Al	6061 Al
Atomization pressure (MPa)	1.21	1.21
Atomization gas	Nitrogen	Nitrogen
Flight distance (mm)	406.4	406.4
Pouring temperature (°C)	750	750
J_{melt}/J_{gas}	2.29	1.97

gas mass flow ratio, J_{melt}/J_{gas}, was the only variable altered during the experiments. The effects of the melt-to-gas mass flow ratio used in experiment 132, relative to that used in experiment 134, on the resulting microstructure will be discussed in a subsequent section.

2.2. Specimen preparation

The geometry of the spray-atomized and deposited 6061 alloy is shown schematically in Fig. 2. In this figure, the orientation of the Z axis was selected to lie in the height direction, whereas the orientations of the X and Y axes were chosen to lie in the short transverse and long transverse directions, respectively. Cantilever beam specimens for damping characterization studies and samples for porosity analyses were simultaneously removed by sectioning the as-spray deposited material into rectangular bars. The following procedure was adopted in order to keep track of the precise location of each sample within the spray-deposited material. The central core of the deposit was first sectioned into a block with the following approximate dimensions: 150 mm long, 70 mm wide and 60 to 80 mm high. This block was subsequently sectioned into several layers along the height direction, and each layer was then divided into rectangular samples. This procedure is shown schematically in Fig. 3 for experiments 132 and 134. In this figure, the relative location of each rectangular specimen inside the spray-deposited block is designated by a number. Every rectangular sample was subsequently divided into two pieces; one was used for the damping measurements, and the other for porosity analyses (Fig. 4). The dimensions of the damping specimens were 101.6 mm long, 12.7 mm wide and 2.54 mm thick. The procedure allowed careful analysis of the microstructure present in the damping specimens, since the microstructure of spray-atomized and deposited materials has been reported to change with spray deposition thickness (Z axis), but remain relatively constant along the longitudinal dimension (Y axis) [18, 19].

2.3. Porosity characterization

Quantitative characterization of the porosity present in the spray-deposited materials was accomplished by means of density measurements and computerized analysis of metallographic samples using an Imageset

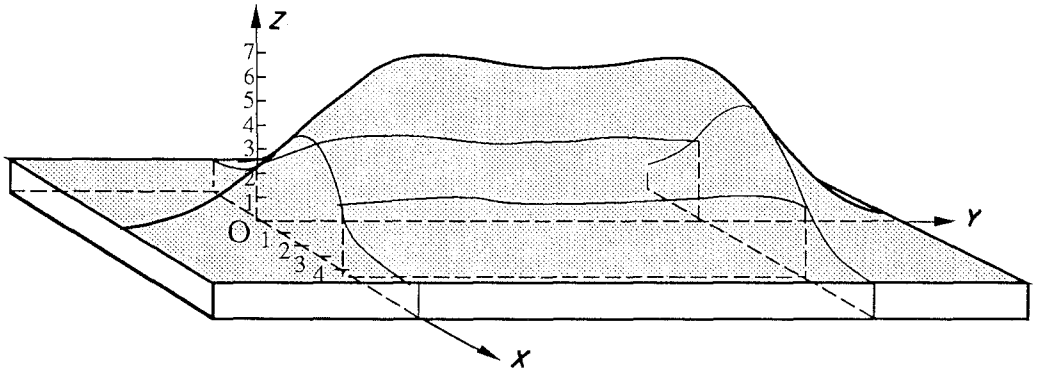

Figure 2 Schematic diagram showing the geometry of the as-spray-deposited 6061 aluminium alloy.

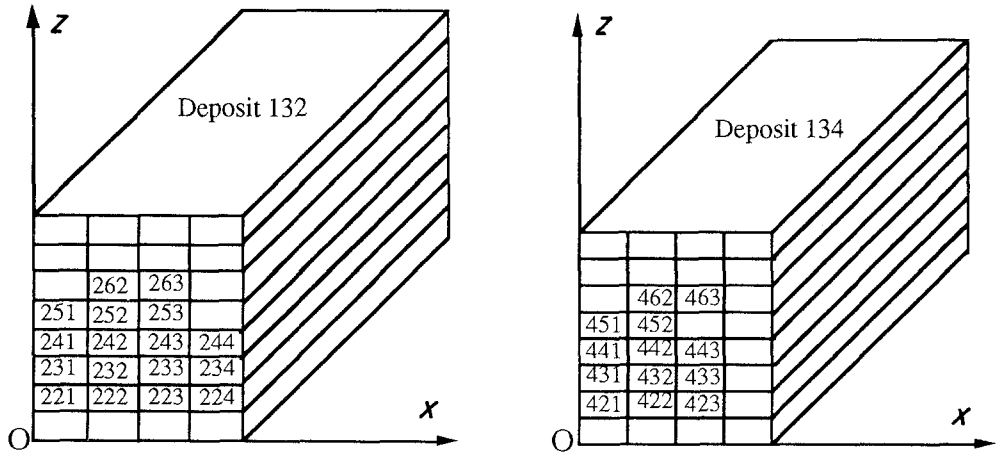

Figure 3 Schematic diagram showing position of samples within the as-spray-deposited materials.

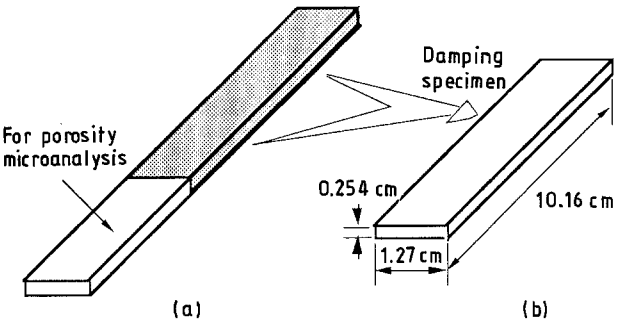

Figure 4 Schematic diagram showing specimen configuration and geometries.

image analyser. The density measurements were conducted in accordance with ASTM B311–83 standard, based on Archimedes' principle. In this procedure the weight of each specimen in air and in liquid was obtained using a Fisher Scientific A-250 electronic balance. The liquid used in the present study was ethylene glycol with a density of 1.113 g cm^{-3} at room temperature (25 °C). Accordingly, the density of a specimen is calculated from the equation

$$\rho_s = \frac{m_{sa}\rho_l}{m_{sa} - m_{sl}} \quad (1)$$

where ρ_s and ρ_l denote the density of the specimen and the liquid, respectively, and m_{sa} and m_{sl} denote the mass of specimen in air and in liquid, respectively. It then follows that the amount of porosity present in each spray-deposited sample can be determined from

$$P = \frac{\rho_{Al} - \rho_s}{\rho_{Al} - \rho_{gas}} \quad (2)$$

where P denotes the volume fraction of porosity present in the sample material, ρ_{Al} represents the theoretical density of 6061 Al and ρ_{gas} represents the density of any inert gas that might be present inside the pores. In the present study, the density of extruded 6061 Al was used as the theoretical density ρ_{Al}, and determined according to the following procedure. A 25.4 mm diameter billet was removed from the as-spray-deposited 6061 Al, and extruded into a rod of 12.7 mm in diameter under 27.58 MPa and at 400 °C. The density of the extruded material was then determined according to Equation 1 as $\rho_{Al} = 2.73$ g cm^{-3}. This value compares favourably with the measured density of 2.72 g cm^{-3} for the as-received 6061-T6 aluminium alloy. Based on the fact that ρ_{gas} is substantially smaller than ρ_{Al} and can be ignored in Equation 2, P is calculated from the equation

$$P = \frac{\rho_{Al} - \rho_s}{\rho_{Al}} \quad (3)$$

While the total amount of porosity present in the spray-deposited materials was determined using the procedure described above, the distribution of pore sizes was quantitatively characterized for each specimen by using image analysis in combination with a Nikon Epiphot optical microscope and a Macintosh IIci computer. An adaptor was utilized in the present work to transmit images from the optical microscope directly to the computer, where the size distribution of pore was readily established. This procedure allowed the characterization of a large number of metallographic samples, accurately and efficiently.

2.4. Damping measurements

The cantilever beam technique was used in the present study to characterize the microstructural damping response of the spray-deposited materials. In this technique, one end of a rectangular specimen was fixed while the opposite end was allowed to move freely in response to a mechanically induced displacement or vibration. The damping capacity of the material was then determined from the resulting displacement spectrum, by utilizing the logarithmic decrement and the half-power bandwidth analysis methodologies. In the logarithmic decrement method, a history of amplitude versus time during a free vibration of the cantilever beam specimen was recorded by an oscilloscope through an optical displacement transducer. By measuring the free amplitude decay after excitation, the logarithmic decrement δ can be evaluated from [2]

$$\delta = \frac{1}{n}\ln\left(\frac{A_i}{A_{i+n}}\right) \quad (4)$$

where A_i and A_{i+n} are the amplitudes of the i^{th} cycle and the $(i + n)^{th}$ cycle, respectively, separated by n periods of oscillation (Fig. 5).

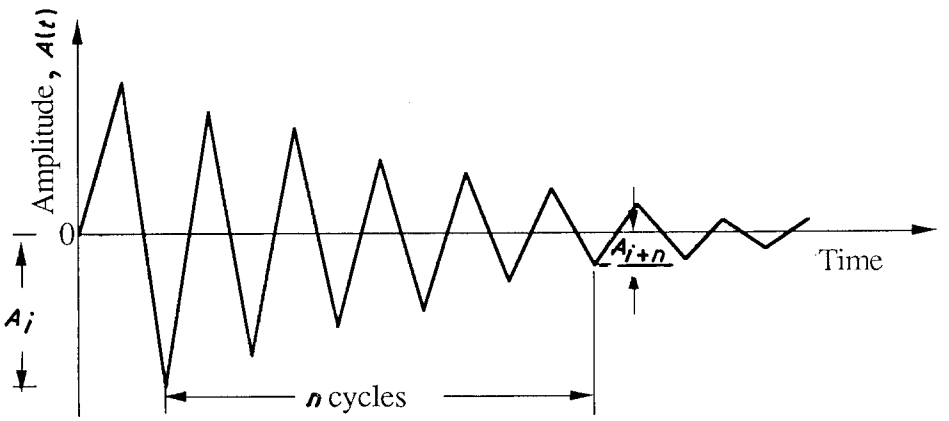

Figure 5 Schematic diagram of free vibration decay [2].

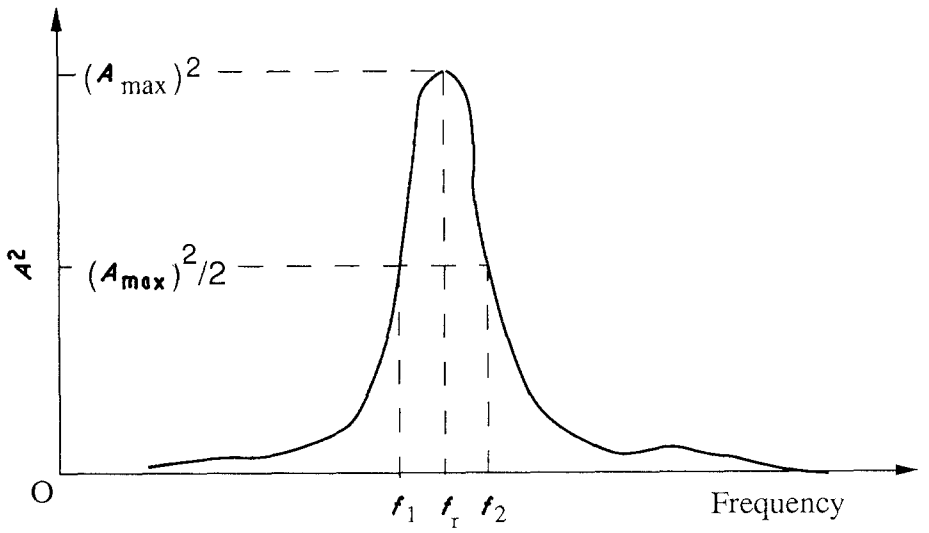

Figure 6 Schematic diagram showing Lorentzian peak.

The half-power bandwidth methodology was based on a forced vibration test in which the specimen was vibrated at the free end by a shaker which was driven by an amplified signal from a white-noise generator. In this technique the resonant frequency peak is distinguished by recording the vibration amplitude as a function of frequency. The inverse qualtity factor or loss factor, Q^{-1}, is then calculated from the vibration spectrum, recorded by a Fast Fourier Transform (FFT) signal analyser through an optical transducer using the equation [2]

$$Q^{-1} = \frac{f_2 - f_1}{f_r} \quad (5)$$

where f_1 and f_2 are the half-power frequencies at which the vibration amplitude is equal to the $2^{-1/2}$ of the maximum amplitude at resonant frequency f_r (Fig. 6). The three frequencies can be readily determined from the Lorentzian peak yielded by plotting the square of amplitude against frequency [2]. Finally, experimental data for the logarithmic decrement δ and the loss factor Q^{-1} can be checked by using the relationship [2, 20]

$$\delta = \pi Q^{-1} \quad (6)$$

All of the damping data used in the present study were derived from experiments performed at the Westinghouse Science and Technology Center (Pittsburgh, Pennsylvania).

3. Results

3.1. Porosity and microstructure

Table II shows the density ρ_s and the amount of porosity P of the as-spray-deposited 6061 Al specimens, calculated from Equations 1 and 3, respectively. The results as shown in Table II correspond to the various locations within the as-spray-deposited materials, as designated in Fig. 3.

Optical microscopy was conducted on unetched and Keller's etched coupons of the as-spray-deposited materials. Two examples, corresponding to experiments 132 and 134, are shown in Figs 7 and 8, respectively. The presence of numerous pre-solidified droplets in the microstructure precluded a precise quantitative assessment of the grain size. However, a large number of observations revealed that the as-spray-deposited grain size ranges from 15 to 49 μm with an average of 32 μm for deposit 132 and from 10 to 35 μm with an average of 22 μm for deposit 134. In addition, the microstructure remained relatively constant throughout the entire specimen length of the as-spray-deposited materials. The evolution of microstructure during spray atomization and deposition has been addressed by numerous investigators, and the interested reader is encouraged to consult the available scientific literature [10, 15, 18].

TABLE II Density and porosity of as-spray-deposited 6061 Al

Deposit	Sample[a]	m_{sa} (g)	m_{sl} (g)	ρ_s (g cm^{-3})	P (%)
132	222	8.5844	4.8565	2.5606	6.20
	242	8.5541	4.8380	2.5597	6.23
	252	8.6848	4.9720	2.6011	4.72
	234	8.3702	4.7875	2.5980	4.83
134	422	8.0587	4.4268	2.4674	9.61
	442	7.5877	4.2314	2.5139	7.91
	452	8.3760	4.6700	2.5132	7.94
	433	8.3339	4.6130	2.4906	8.77

[a] Sample location is shown in Fig. 3.

Size distributions of the pores present in the samples from deposits 132 and 134 are shown in Figs 9 and 10, respectively. In order to quantify the size distribution and morphology of the pores, optical metallography samples were studied using image analysis, in combination with a Nikon Epiphot optical microscope and a Macintosh IIci computer. The results are shown in Table III, where the total amount of porosity present in the samples, as inferred from image analysis, is compared with that obtained using Archimedes' principle. Also shown in Table III is the average diameter of the pores present in the as-spray-deposited microstructure, as determined from image analysis. Each data point shown in Table III was determined by examining two to three viewing areas. This procedure increased the accuracy of the measured values. In

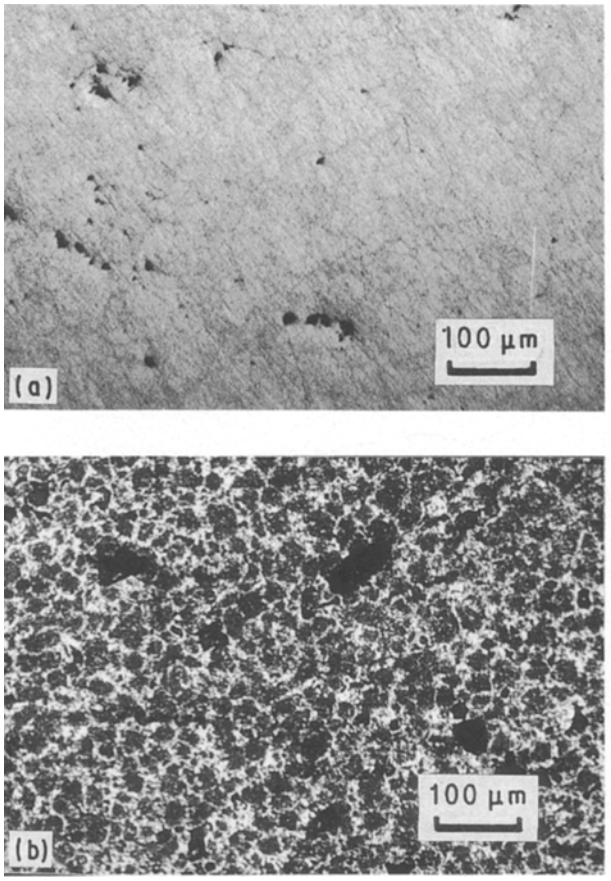

Figure 7 Optical micrographs showing the typical grain and pore morphology present in deposit 132: (a) pore distribution, (b) grain structure.

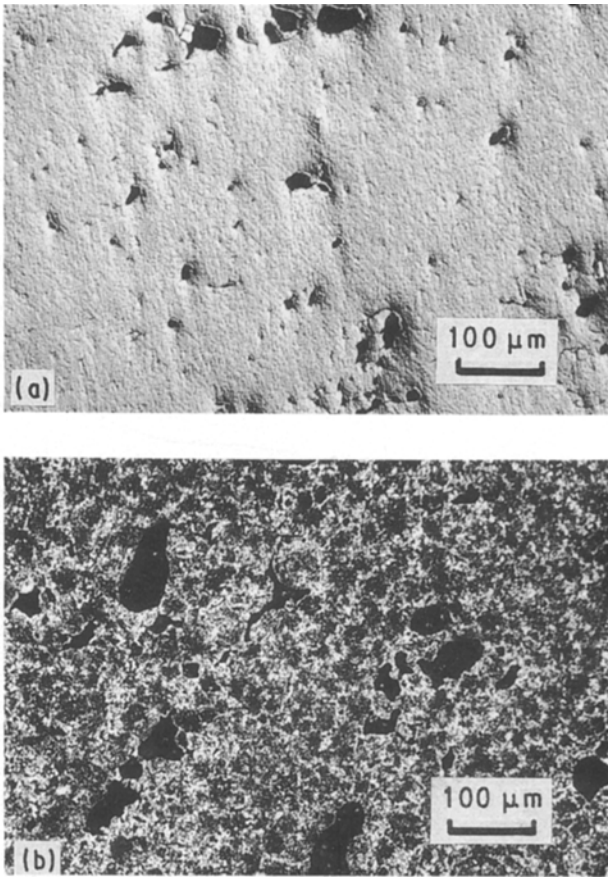

Figure 8 Optical micrographs showing the typical grain and pore morphology present in deposit 134: (a) pore distribution, (b) grain structure.

general, comparison of the amount of porosity present in the spray-deposited materials determined using image analysis and Archimedes' principle revealed a relatively good agreement between both techniques.

3.2. Damping capacity

Experimental results of representative damping specimens for two runs of the as-spray-deposited 6061 aluminium alloy are summarized in Table IV. Also shown in this table are the Lorentzian peak frequencies for each of the samples tested. The free decay vibration tests were performed at a frequency of 290 $\pm$ 10 Hz with the strain amplitude in a range of

TABLE III Porosity of as-deposited 6061 aluminium alloy by image analysis

Run	Sample[a]	P (%) (Image analysis)	P (%) (Archimedes)	d (μm)[b]
132	222	6.45	6.20	5.38
	242	6.90	6.23	3.96
	252	4.80	4.72	2.36
	234	3.78	4.83	1.91
134	422	10.12	9.61	9.30
	442	8.99	7.91	7.32
	452	7.42	7.94	5.51
	433	9.48	8.77	5.50

[a]Sample location is shown in Fig. 3.
[b]Average pore diameter as determined from image analysis.

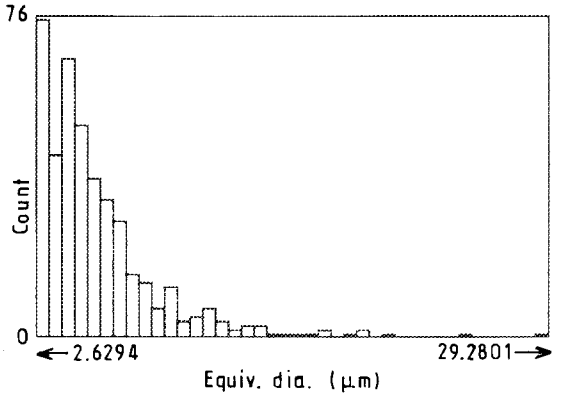

Figure 9 Distribution of pore sizes present in sample 222 from deposit 132 (see Fig. 3): total count = 424, mean = 6·0077, s.d. = 3·3497.

TABLE IV Damping capacity of as-spray-deposited 6061 Al

Deposit	Sample	δ (%)	f_r (Hz)	Q^{-1}(%)
132	222	2.0	294.50	0.7
	242	1.9	292.00	0.6
	252	1.9	300.25	0.6
	234	2.0	287.50	0.7
134	422	2.9	280.75	0.8
	442	2.6	261.25	1.7
	452	1.8	281.25	0.8
	433	2.3	280.50	0.8

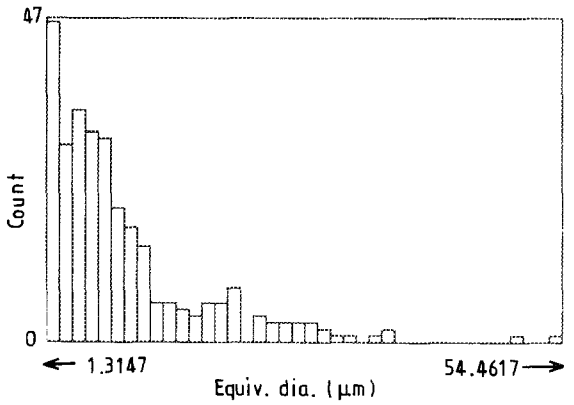

Figure 10 Distribution of pore sizes present in sample 422 from deposit 134 (see Fig. 3): total count = 288, mean = 9.3283, s.d. = 8.2564.

$\pm$ 340 to $\pm$ 60 microstrain. The resonant vibration tests were conducted under the strain amplitude of $\pm$ 20 microstrain over a 240 to 330 frequency range. Comparison of the values of the logarithmic decrement δ with those of the loss factor Q^{-1}, using Equation 6 suggests good agreement between the logarithmic decrement and the half-power bandwidth techniques. One notable exception to this observation is the result obtained for sample 442 from deposit 134, which shows that the loss factor for this sample was abnormally high (1.7%). This was attributed to difficulties with the experimental measurements.

4. Discussion

4.1. Formation of porosity

In order to discuss the effects of porosity on damping behaviour it is first necessary to provide some background information on the factors that govern the formation of pores during spray-atomization and deposition. This background information will also provide a basis for the discussion on the differences in the size and distribution of pores present in the materials obtained from deposits 132 and 134. Both Table III and Fig. 11 show that there was a relatively close correlation between the amount of porosity present and the average pore size. Therefore, in the discussion that follows, average pore size and amount of porosity may be thought of as interchangeable terms.

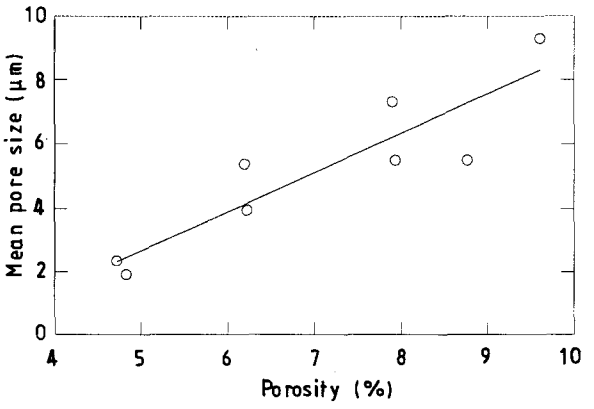

Figure 11 Relationship between mean pore size and porosity for as-spray-deposited 6061 Al alloy.

An important microstructural characteristic frequently associated with the microstructure of the as-spray-atomized and deposited materials is the presence of a finite amount of non-interconnected pores [9–15, 18, 19, 21, 22]. The overall amount of porosity present in spray-atomized and deposited materials depends on: (a) the thermodynamic properties of the material, (b) the thermodynamic properties of the gas, and (c) the processing parameters. Under conditions typical for aluminium alloys, for example, the amount of porosity present in spray-atomized and deposited materials has been reported to be in the 1 to 10% range [13, 14, 18]. This is consistent with the results of the present study which showed porosity levels in the 4 to 10% range. Furthermore, the present results also revealed that the size distribution of pores was skewed (see Figs 9 and 10), with an average pore diameter in the 6 to 10 μm range.

The origin of porosity in spray-atomized and deposited materials may be attributed to one or a combination of the following mechanisms: (a) gas rejection, (b) solidification shrinkage, (c) interparticle porosity. The first mechanism, gas rejection, is anticipated as a result of the limited solid solubility of inert gases in most structural materials. As the temperature of the material decreases during solidification, any amount of gas that might have dissolved during the melting and superheating stage will be rejected into the matrix, leading to the formation of gas pores. However, results obtained using fast neutron activation analyses show that spray-atomized and deposited materials exhibit extremely low levels of dissolved gases, suggesting that this mechanism is not as important as originally suggested [23]. In addition, in view of the irregular morphology of the pores, it is highly improbable that a large proportion of the porosity originates from the rejection of entrapped gases, since gas porosity generally exhibits a spheroidal morphology (see Figs 7 and 8).

The formation of shrinkage porosity is generally associated with sluggish solidification kinetics, such as those present during ingot casting. In view of the limited amount of liquid phase present under normal spray-atomization and deposition conditions, it is unlikely that solidification shrinkage plays an important role in the formation of the observed pore distribution [12–14]. It is worth noting, however, that if the spray-atomization and deposition conditions are such that there is an excessive amount of liquid phase present at the deposition surface, this mechanism may play a significant role in the formation of porosity. The presence of an excess amount of liquid phase during impact may develop as a result of (a) coarse droplet sizes, (b) high deposition temperatures, and (c) remelting of solid phases caused by high spray enthalpies [13, 14]. Under these conditions, the atomization gas may interact with the molten metal, leading to the formation of large amounts of porosity.

The available experimental evidence suggests that a large proportion of the porosity that is generally observed in spray-atomized and deposited materials may be attributed to the third mechanism, interparticle porosity. As the droplets descend, first on the

deposition surface, and eventually on each other, they overlap leaving micrometre-sized cavities in between. In spite of the large amount of turbulence present, the relatively rapid drop in temperature during deposition prevents any liquid phase present from filling all of the cavities, leading to the formation of irregular pores. This mechanism is consistent with the observed correlation between deposition conditions such as spray density, powder size, and the amount of porosity present throughout the deposit. For example, the higher density associated with the central region of the deposit may be attributed to the elevated mass flux of droplets in the region of the spray, relative to the periphery [19]. These droplets contain elevated fractions of liquid phase, effectively filling the interstices between droplets. Regarding the variations in density as a function of thickness, the present results show that the highest amount of porosity present in the spray-deposited materials was present in the samples closest to the water-cooled substrate (samples 222 and 422 in Table III). This is consistent with the initially high rates of heat extraction experienced by the region of the deposit in close proximity to the substrate. In contrast, the high amount of porosity generally observed in the periphery of the samples (samples 234 and 433) results from a large proportion of small, pre-solidified droplets that tend to segregate to this region. It is noticed that under the processing conditions where deposited droplets are allowed to solidify completely before the arrival of more droplets, interlayer porosity will also develop at the original droplet boundaries.

In order to establish a relationship between the amount of porosity present and the processing parameters, it is useful to consider the factors governing the atomization stage of the process. The disintegration of a molten metal by high-energy gas jets (atomization) is complex and only portions of it have been addressed from a theoretical viewpoint [24, 25]. The work of Lubanska [25] showed that the disintegration of liquids by high-velocity jets obeys a simple correlation. A slightly modified form of the original correlation has been shown to represent the results of molten metal atomization experiments reasonably well [12, 21, 22]. According to the modified Lubanska's correlation, the mass mean droplet diameter (i.e. the opening of a screening mesh which lets through 50% of the mass of the powder resulting from an atomization experiment), d_{50}, is given by

$$d_{50} = K_d\left[\left(1+\frac{J_{melt}}{J_{gas}}\right)\left(\frac{\mu_m d_0 \sigma_m}{\mu_g V_{ge}^2 \rho_m}\right)\right]^{1/2} \quad (7)$$

where K_d is an empirically determined constant with a value between 40 and 400; a value of 51.7 was selected for the conditions used in the present study, since this has been shown to yield a good correlation between theory and experiment [26]; μ_m, σ_m, ρ_m and J_{melt} are the viscosity, surface tension, density and mass flow rate of the melt, respectively; μ_g, V_{ge} and J_{gas} are the viscosity, velocity and mass flow rate of the atomizing gas, respectively; and d_0 is the diameter of the metal delivery nozzle. Expressions for the flow rates can be obtained as functions of the process parameters from Bernoulli's equation in the case of the metal [27] and from the theory of compressible flow [28] in the case of the gas. The mass mean droplet diameter of the powder size distribution (d_{50}) for both experiments was computed from Equation 7, using the processing parameters and physical constants corresponding to each experiment (see Table I and Table V). Equation 7 predicts d_{50} values of 108 and 98 μm for deposits 132 and 134, respectively. These results are consistent with the higher densities that were noted for deposit 132, relative to those of deposit 134, since a smaller droplet diameter will dissipate thermal energy more effectively, thereby leading to a greater extent of pre-solidification prior to impact.

4.2. Relationship between porosity and damping

The damping capacity of the as-spray-atomized and deposited 6061 aluminium alloy obtained in the present study is summarized in Table VI, where the values of the logarithmic decrement δ are compared with the results obtained by other investigators using the same alloy. The values of δ shown in Table VI were the average of the four samples investigated for each deposit (see Table IV). The results show that the value of δ for as-spray-deposited 6061 Al is higher than those reported by other investigators. The damping response of the as-spray-deposited 6061 Al is thought to be derived from two factors: (a) the presence of a finite amount of micrometre-sized pores, and (b) a fine-grained microstructure. In the discussion that follows, this suggestion is discussed with reference to results reported by other investigators.

Previous studies [3–5] demonstrated that the damping capacity of an impregnated porous non-metallic material increases with amount of porosity, concomitant with a drop in elastic modulus and strength. This observation is substantiated by the results obtained for 6061 Al alloy processed by spray-

TABLE V Computational d_{50} for two deposits of 6061 Al[a]

Deposit	d_0 (cm)	J_{gas} (g s^{-1})	J_{melt} (g s^{-1})	d_{50} (μm)
132	0.3048	9.87	22.58	108
134	0.2794	9.87	19.46	98

[a] Gas: nitrogen with $\mu_g = 1.54 \times 10^{-4}$ g cm^{-1} s^{-1},
$\rho_{gas} = 3.375 \times 10^{-3}$ g cm^{-3},
$V_{ge} = 3.232 \times 10^4$ cm s^{-1};
$K_d = 51.7$;
melt: 6061 Al with
$\mu_m = 1.3 \times 10^{-2}$ g cm^{-1} s^{-1},
$\rho_m = 2.385$ g cm^{-3},
$\sigma_m = 914$ g s^{-2}.

TABLE VI Comparison of damping behaviour of 6061 with results of other studies

Processing	Reference	f (Hz)	δ(%)
As-deposited, run 132	This work	290	1.95 ± 0.05
As-deposited, run 134	This work	280	2.40 ± 0.47
6061-T6	[16]	500	0.62
6061-T6	[17]	15	1.82
6061-0	[20]	19.8	0.65

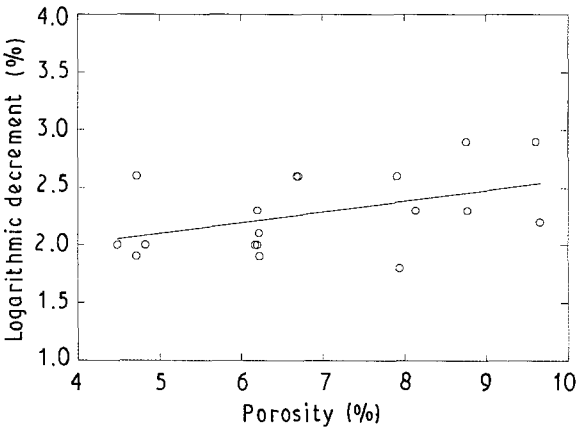

Figure 12 Relationship between damping capacity and porosity for as-deposited 6061 Al alloy.

atomization and deposition in the present study, as shown in Fig. 12. The results shown in this figure suggest that the value of the logarithmic decrement δ increases with increasing porosity present in the 6061 Al alloy, although the data points for the damping specimens were somewhat scattered. The scattering that is evident from Fig. 12 was attributed to the slight variations in microstructure that were present in the samples investigated. The relationship between porosity and mean pore size for the samples is shown in Fig. 11. It is seen that the amount of porosity is proportional to the average pore size. Fig. 13 shows two typical pore size probability distributions from deposits 132 and 134, as determined by image analysis (see Figs 9 and 10). The results in Fig. 13 reveal that even though there was no difference in the pore size below the tenth percentile of the pores (d_{10}, the opening of a screening mesh which lets through 10% of the mass of the powder) between both runs of the as-spray-deposited 6061 Al alloy, the difference in the ninetieth percentile of pores (d_{90}, the opening of a screening mesh which lets through 90% of the mass of the powder) was substantial. d_{90} was 10.1 μm for sample 222 from deposit 132 and 19.1 μm for sample 422 from deposit 134. On the basis of these observations, the larger pores inside the as-spray-deposited 6061 aluminium alloy appear to play a more important role in damping behaviour than the smaller pores.

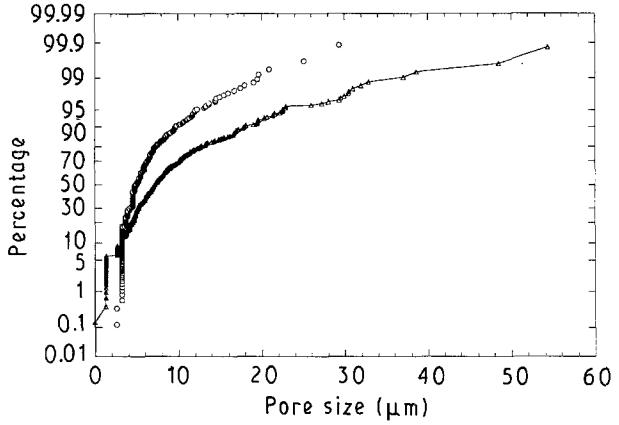

Figure 13 Typical distributions of pore sizes in as-spray-deposited 6061 Al alloy (see Fig. 3 for sample identification numbers). (○) Sample 222; $d_{10} = 3.21$, $d_{90} = 10.1$. (△) Sample 422; $d_{10} = 3.21$, $d_{90} = 19.1$.

The dissipation of elastic energy in porous materials has been rationalized in terms of a mechanism known as mode conversion [29–31]. From a microscopic viewpoint, every point inside a cantilever beam specimen under lateral vibration will move in a transverse direction. Hence, every crystal or grain deforms in shear due to the transverse motion of the specimen and in tension and shear due to the non-uniform deformation along the longitudinal direction of the cantilever beam. In a porous metal, the stress state may change from tensile stress into shear stress at the boundaries of pores. The shear deformation may furthermore produce viscoelastic flow that is most readily achieved at the pore boundaries. The viscous flow is then converted to heat by molecular collisions or dislocations during cyclic movement. The production of either thermal energy or dislocations is beneficial to internal friction or material damping according to thermodynamics [32] and Granato–Lucke dislocation theory [33, 34], respectively. The eventual result of these serial conversions is the decay of vibration of the porous material. The mode conversion changes normal stress into shear stress at pore boundaries and therefore increases the probability and density of dislocations around the pores, thereby increasing the damping capacity due to internal friction. In addition, the movements of dislocations tend to end at pore surfaces where there is high surface energy converted from dislocation mobility, and therefore pores may be high-energy dissipation resources. It is also worth noting that on the basis of the present experimental results, the mode conversion effect appears to be more pronounced around large pores (see Figs 11 and 12).

Mode conversion may be also partially reached when there is a certain medium inside the pores [29]. The spray-atomized and deposited 6061 alloy used in the present study was processed in an inert gas atmosphere. Inside the deposited 6061 aluminium alloy, the low solubility of the atomizing gas may lead to the formation of some pores containing a partial pressure of inert gas. In this case the motion of the inert gas relative to the porous framework material will be high, since the porous material is rigid in comparison with the inert gas [12–14]. As a consequence, there will be an impedance mismatch to vibration movement between the inert gas and the as-spray-deposited metal. This mismatch may change the deformation field in the neighbouring metal region and therefore lead to secondary shear deformation in the neighbouring metal, increasing the density of dislocations, and thereby the damping due to internal friction.

4.3. Effect of grain size on damping

Fine grain morphology is one of the characteristics of spray-atomized and deposited metals and alloys. The average grain size of the as-spray-deposited 6061 aluminium alloy was 32 μm for sample 222 from deposit 132 and 22 μm for sample 422 from deposit 134; both were much smaller than the 73 μm of the as-received 6061-T6 aluminium alloy [35]. Damping associated with grain boundary relaxation, anelasticity or viscosity in the polycrystalline metals has been described

by kê [36], Zener [37], and Nowick and Berry [2], respectively. In polycrystalline metals there exist amorphous grain boundaries that display viscous-like properties. The viscous flow at grain boundaries will convert mechanical energy produced under cyclic shear stress into thermal energy, as a result of internal friction. The thermal energy will then be dissipated by the conductivity of the metal and by heat exchange with the surroundings. The energy absorbed in grain boundaries not only depends on the magnitude of the shear stress and the anelastic shear strain, but also is proportional to the grain boundary area per unit volume, i.e. inversely proportional to grain size [36–38]. In view of these results, the fine-grained microstructure of the spray-atomized and deposited 6061 aluminium alloy may also play an important role in the dissipation of elastic strain energy.

5. Conclusions

The spray-atomization and deposition processing technique can be used to produce a metal or alloy with a pre-determined amount of non-interconnected, micrometre-sized pores. The damping characterization results of the present work show that the presence of micrometre-sized pores increases the damping capacity of the as-spray-atomized and deposited 6061 aluminium alloy. The damping capacity, in terms of logarithmic decrement δ of the 6061 aluminium processed by spray-atomization and deposition, is higher than that reported by other investigators using other processing techniques on the same alloy. The damping characteristics of the spray-deposited material obtained in the present work are thought to be derived from two factors: (a) the presence of a finite amount of micrometre-sized pores, and (b) a fine-grained microstructure. Damping mechanisms may be associated with porosity by stress mode conversion and resultant dislocation damping at pores and with a refined grain morphology by grain boundary sliding.

Acknowledgements

The authors wish to acknowledge the financial support of the Office of Naval Research (Grant No. N00014-90-J-1923 to the University of California at Irvine, and Grant No. N00014-90-C-0211 to the Westinghouse Science and Technology Center). In addition, the authors would also like to express their gratitude to C. Wong of David Taylor Research Center, for her able technical assistance and valuable discussions; to E. S. Diaz of the Westinghouse Science and Technology Center, and to I. Sauer of the University of California at Irvine for their assistance.

References

1. B. J. LAZAN, "Damping of Materials and Members in Structural Mechanics" (Pergamon, Oxford, 1968) p. 38.
2. A. S. NOWICK and B. S. BERRY, "Anelastic Relaxation in Crystalline Solids" (Academic, New York, 1972) pp. 18, 21, 436.
3. K. SHIMIZU, in "Composite Materials; Mechanics, Mechanical Properties and Fabrication", edited by K. Kawata and T. Akasaka (Japan Society for Composite Materials, Tokyo, 1981) p. 111.
4. T. KLIMENTOS and C. McCANN, *Geophysics* **55** (1990) 998.
5. L. F. NIELSEN, *J. Amer. Ceram. Soc.* **67** (1984) 93.
6. R. W. RICE, *Mater. Sci. Eng.* **A112** (1989) 215.
7. S. M. KAUFMAN and S. MOCARSKI, *Int. J. Powder Metall.* **7** (1971) 19.
8. S. M. KAUFMAN, *ibid.* **8** (1972) 183.
9. P. S. GRANT, W. T. KIM, B. P. BEWLAY and B. CANTOR, *Scripta Metall.* **23** (1989) 1651.
10. A. L. MORAN, and W. A. PALKO, *J. Metals* **40** (Dec. 1988) 12.
11. P. MATHUR, D. APELIAN and A. LAWLEY *Acta Metall.* **37** (1989) 429.
12. E. GUTIERREZ-MIRAVETE, E. J. LAVERNIA, G. TRAPAGA, J. SZEKELY and N. J. GRANT, *Metall. Trans.* **20A** (1989) 71.
13. E. J. LAVERNIA, *Int. J. Rapid Solidif.* **5** (1989) 47.
14. M. GUPTA, F. A. MOHAMED and E. J. LAVERNIA *ibid.* **6** (1991), 247.
15. E. J. LAVERNIA, T. ANDO and N. J. GRANT, in "Rapidly Solidified Materials", edited by P. Lee and R. Carbonara (ASM, Materials Park, Ohio, 1985) p. 29.
16. R. B. BHAGAT, M. F. AMATEAU and E. C. SMITH, in "Cast Reinforced Metal Composites", edited by S. G. Fichman and A. K. Dhingra (ASM, Materials Park, Ohio, 1988) p. 399.
17. M. S. MISRA and P. D. LaGRECA, in Proceedings of Vibration Damping Workshop, Long Beach, California, February 1984, edited by L. Rogers, AFWAL-TR-84-3064 (1984) p. U-1.
18. B. P. BEWLAY and B. CANTOR, in "Rapidly Solidified Materials", edited by P. Lee and R. Carbonara (ASM, Materials Park, Ohio, 1986) pp. 15.
19. V. G. McDONELL, E. J. LAVERNIA and G. S. SAMUELSEN, in "Synthesis and Analysis in Materials Processing: Advances in Characterization and Diagnostics of ceramic and Metal Particulate Processing", edited by E. J. Lavernia *et al.* (Metallurgical Society, 1989) p. 13.
20. G. G. WREN and V. K. KINRA, "Damping in Metal Matrix Composites: Theory and Experiment", Technical Report (Texas A&M University, 1990) pp. 19, 140.
21. E. J. LAVERNIA, E. GUTIERREZ-MIRAVETE, J. SZEKELY and N. J. GRANT, *Progr. in Powd. Metall.* **43** (1987) 683.
22. R. VETTER, L. Z. ZHUANG, I. MAJEWSKA-GLABUS and J. DUSZCZYK, *Scripta Metall. Mater.* **24** (1990) 2089.
23. K. OGATA, E. J. LAVERNIA, G. RAI and N. J. GRANT, *Int. J. Rapid Solidif.* **2** (1986) 21.
24. T. MIKAMI, R. G. COX and S. G. MASON, *Int. J. Multiphase Flow* **2** (1975) 113.
25. H. LUBANSKA, *J. Metals* **22** (Feb. 1970) 45.
26. X. ZENG, thesis for MSc in Engineering, University of California, Irvine, (1992).
27. G. H. GEIGER and D. R. POIRIER, "Transport Phenomena in Metallurgy" (Addison-Wesley, Reading, Massachusetts 1973) p. 134.
28. A. H. SHAPIRO, "The Dynamics and Thermodynamics of Compressible Fluid Flow," Vol. 1 (Ronald, New York, 1953) p. 85.
29. J. JARZYNSKI, in "Sound and Vibration Damping with Polymers," edited by R. D. Corsaro and L. H. Sperling (American Chemical Society, Washington, DC, 1990) p. 167.
30. R. D. CORSANO, J. F. COVEY, R. M. YOUNG and G. SPRYN, *ibid.* p. 208.
31. W. M. MADIGOSKY and K. P. SHARNHORST, *ibid.* p. 228.
32. D. ZHANG and B. I. SANDOR, *Fatigue Fract. Eng. Mater. Struct,* **13** (1990) 497.
33. A. GRANATO and K. LUCKE, *J. Appl. Phys.* **27** (1956) 583.
34. *Idem, ibid.* **27** (1956) 789.
35. R. J. PEREZ, J. ZHANG and E. J. LAVERNIA, in Proceedings of Advanced Materials Symposium, ISTFA 91, Los Angeles, November 1991 (ASM, 1991).
36. C. ZENER, "Elasticity and Anelasticity of Metals" (University of Chicago Press, Chicago, 1948) p. 147.
37. M. TANAKA and H. IIZUKA, *J. Mater. Sci.* **26** (1991) 4389.

Received 2 October 1991
and accepted 11 August 1992